Andean Geology 42 (2): 190-212. May, 2015
doi: 10.5027/andgeoV42n2-a03

Andean Geology
www.andeangeology.cl

Deglacial ice-marginal glaciolacustrine environments and structural moraine building in Torres del Paine, Chilean southern Patagonia

***Juan-Luis García[1,4], Jorge A. Strelin[2], Rodrigo M. Vega[3], Brenda L. Hall[4], Charles R. Stern[5]**

[1] *Current address: Instituto de Geografía, Facultad de Historia, Geografía y Ciencia Política, Pontificia Universidad Católica de Chile, Avda. Vicuña Mackenna 4860, Santiago.*
jgarciab@uc.cl

[2] *Instituto Antártico Argentino, CICTERRA, Universidad Nacional de Córdoba, X5016GCA, Córdoba, Argentina.*
jstrelin@yahoo.com.ar

[3] *Instituto de Ciencias de la Tierra y Evolución, Avda. Eduardo Morales Miranda s/n, Campus Isla Teja, Universidad Austral de Chile, Valdivia, Chile.*
rmvega@uach.cl

[4] *School of Earth and Climate Sciences and Climate Change Institute, University of Maine, Orono ME 04469, USA.*
brendah@maine.edu

[5] *Department of Geological Sciences, University of Colorado, CB399, Boulder, Colorado 80309-0399, USA.*
charles.stern@colorado.edu

* *Corresponding author: jgarciab@uc.cl*

ABSTRACT. The late-glacial sedimentologic and geomorphic record of the former Patagonian ice sheet remains mostly unstudied despite the fact that it affords invaluable evidence for glaciologic processes during the last glacial-interglacial transition (*i.e*., 18-11.5 ka). This information is critical if landforms (*e.g*., moraines) and associated sediments are to be used for paleoclimate reconstruction. El Canal stratigraphic section in Torres del Paine, southern Chile (51ºS), provides one of the few complete late-glacial morphostratigraphic records preserved on land in Patagonia that has not been reworked by postglacial lake or marine transgressions. Therefore, it provides unique evidence for reconstructing former environments, processes and fluctuations along the ice front at the end of the last glaciation. Here, we present results of a morphostratigraphic study of this site, which was shaped during the late-glacial Torres del Paine-TDP II, III and IV glacier fluctuations. We document the presence of eight sediment lithofacies associations and six stratigraphic sections that expose a complete record of proximal to distal subaqueous processes, which we link to phases of glacier advance (*e.g*., moraine building) and retreat. During the late-glacial, the Lago del Toro ice lobe pushed and glaciotectonized ice-contact lake sediments several times to shape the TDP moraine ridges fringing present-day lake. The saw-toothed morphology of the ridges confirms the structural origin of these landforms. Based on sediment facies associations, we conclude that local glacial lakes developed along the ice front during deposition of the late-glacial TDP II-IV moraine belts, suggesting that collapse, and associated continental drainage diversion, of major regional-size lakes in Torres del Paine had occurred during this time.

Keywords: Glaciolacustrine sediments, Push moraines, Late-glacial, Torres del Paine National Park, Patagonian paleolakes, Patagonian Ice Sheet.

RESUMEN. Ambientes glaciolacustres y construcción estructural de morrenas frontales tardiglaciales en Torres del Paine, Patagonia austral chilena. El registro sedimentológico y geomorfológico tardiglacial del antiguo hielo continental Patagónico permanece poco estudiado, a pesar de representar una invaluable información glaciológica de la última transición glacial-interglacial (18 a 11,5 ka). La definición de los atributos físicos de morrenas y sedimentos depositados durante este período es importante para así evaluar su potencial como indicadores de paleoclima. La sección estratigráfica de El Canal en las afueras del parque nacional Torres del Paine, al sur de Chile (51ºS), ofrece uno de los pocos registros morfoestratigráficos tardiglaciales completos y bien preservados de la Patagonia, no afectados por transgresiones marinas o lacustres posglaciales. Este registro, por lo tanto, proporciona evidencia única para la reconstrucción glaciológica de los antiguos márgenes del hielo Patagónico, sus procesos asociados y las fluctuaciones del frente de hielo al final de la última glaciación. En este trabajo presentamos los resultados de un estudio morfoestratigráfico basado en la evidencia del sitio El Canal, formado cuando el lóbulo glacial Lago del Toro depositó las morrenas tardiglaciales Torres del Paine-TDP II, III y IV. Aquí documentamos la presencia de ocho litofacies de asociaciones de sedimentos y seis secciones estratigráficas que exponen un registro completo de ambientes subacuáticos que incluyen desde aquellos en contacto, proximales y distales al frente del hielo, evidenciando procesos de avance (construcción de morrenas) y retroceso glacial. Durante el período tardiglacial el lóbulo glacial Lago del Toro empujó y glaciotectonizó los sedimentos glaciolacustres proximales al hielo en variadas ocasiones para formar los cinturones morrénicos TDP que bordean el actual lago del Toro. La morfología aserrada de las crestas morrénicas confirma el origen estructural de estas geoformas. Sobre la base de las asociaciones de sedimentos presentes, concluimos que lagos glaciales de extensión local se desarrollaron a lo largo del frente de hielo durante la deposición de los cinturones morrénicos TDP II-IV, aspecto que sugiere que el colapso de los lagos de tamaño regional en la cuenca de Torres del Paine, y el cambio en la dirección del drenaje continental asociado, ya se había producido durante este período.

Palabras clave: Sedimentos glaciolacustres, Morrenas de empuje, Tardiglacial, Parque Nacional Torres del Paine, Paleolagos de la Patagonia, Campos de Hielo Patagónico.

1. Introduction

A complete record of late-glacial features and environments at the former Patagonian Ice Sheet margin, including sedimentologic and morphologic data within a precise chronological framework, is required to assess past ice-front dynamics and paleoclimate variability at the end of the last glaciation. The Patagonian region exposes exceptionally well-preserved Quaternary sediments and landforms (*e.g*., Caldenius, 1932; Sugden *et al*., 2005; Kaplan *et al*., 2005; Glasser *et al*., 2008; Hein *et al*., 2009; Strelin *et al*., 2011; García, 2012; García *et al*., 2014). However, well-preserved late-glacial landforms and sediments are not widespread, because they commonly are at least partially inundated by deep lakes and marine inlets. In this work, we provide a detailed description of the late-glacial morphostratigraphic record of the former Lago del Toro ice lobe (Marden and Clapperton, 1995; García *et al*., 2014) in the Torres del Paine National Park surroundings, Chilean Patagonia (51ºS; 73ºW).

This research focuses on a stratigraphic section known as El Canal, located at the eastern coast of Lago del Toro (Caldenius, 1932; Marden, 1993; Solari *et al*., 2012; Fig. 1). This study sector is one of the few sites in Patagonia where the entire late-glacial morphostratigraphic record is preserved on land (García *et al*., 2012) and is therefore suitable for sedimentological investigations in order to aid paleoenvironmental reconstructions. About a hundred years ago, a two-kilometer long, west-east trench was artificially deepened at this location, within a natural glacial meltwater channel that cuts the Torres del Paine (TDP) I to IV end moraines deposited by the Lago del Toro ice lobe at the end of the last glaciation (Marden and Clapperton, 1995; García *et al*., 2012; García *et al*., 2014). Historically, El Canal has been used to divert spring meltwater from Las Chinas River into Lago del Toro, which has resulted in erosion and sediment exposures as much as 20 m high. As a consequence, El Canal and surrounding glacial geomorphology exposes a complete morphostratigraphic record useful to reconstruct local ice-marginal environments and associated processes at the end of the last glaciation. Here, we use geomorphic and sedimentologic evidence to determine the formation of terminal landforms, building on previous models of moraine depositional processes (*e.g*., Boulton, 1986; Turbek and Lowell, 1999; Bentley, 1996; Mager and Fitzsimons, 2007). Knowledge of the glacial processes linked to moraine construction is important, particularly as these landforms are used to develop paleoclimate records (Marden and Clapperton, 1995; García *et al*., 2012).

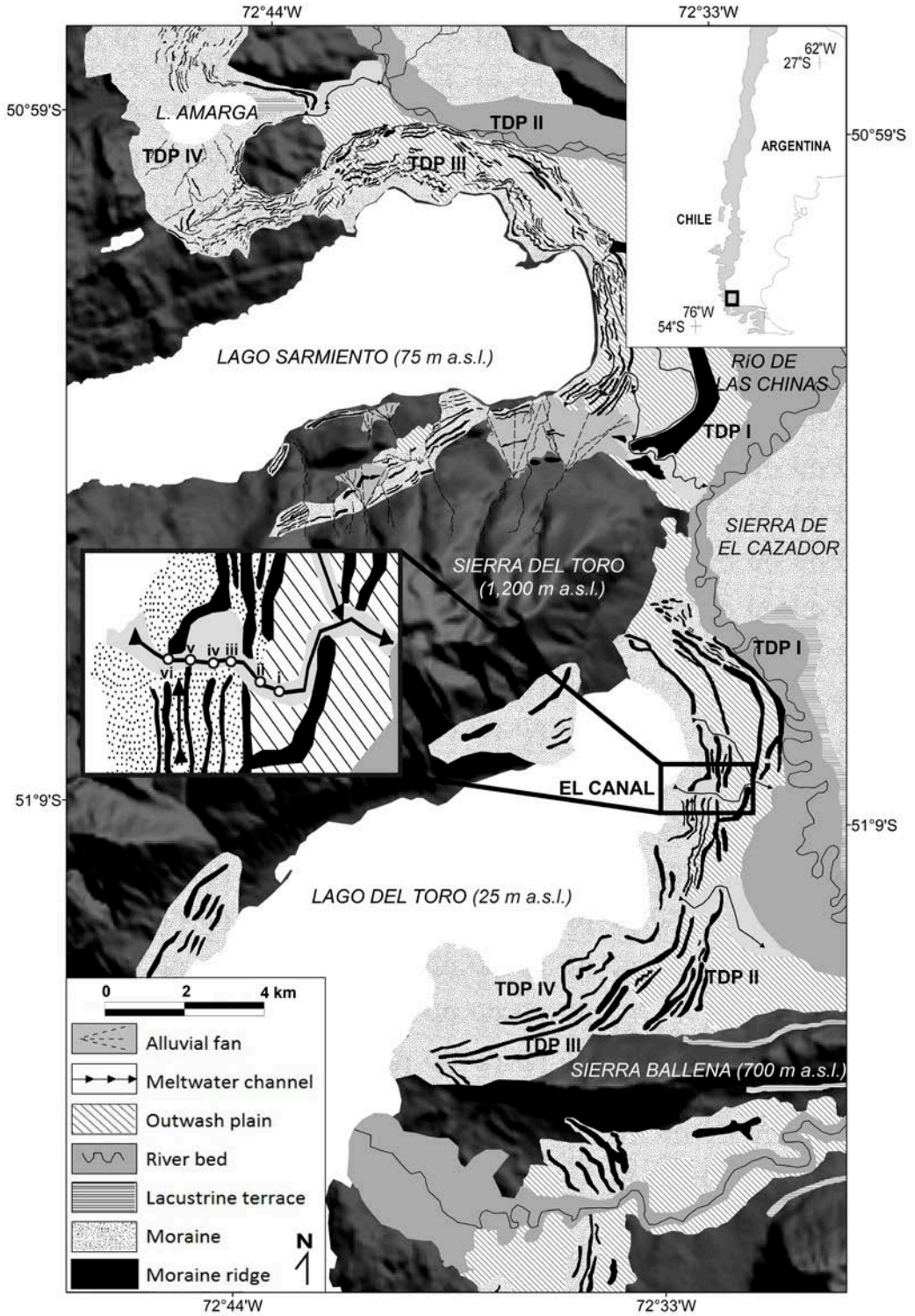

FIG. 1. Map of Lago Sarmiento and Lago del Toro with main glacial geomorphic elements displayed (modified from García *et al*., 2014). Inset at the center of main map encloses the El Canal meltwater channel study area, which is shown enlarged with the six stratigraphic sections discussed in the text. Elevations are approximate. Ice flowed from the west.

1.1. Physical Setting

The study area has a cold, temperate climate, with marked thermal and precipitation gradients across the Andes. At present, the core of the westerly wind belt intersects South America at about 50ºS and is associated with high precipitation (as much as 10 m per year at the Southern Patagonian Ice Field) and low temperatures that directly affect the regional climate and glacier mass balance. The Torres del Paine field area is situated in the lee of the Andes adjacent to the southeastern margin of the Southern Patagonian Ice Field and corresponds to a transition from deciduous forest to the west and a semi-arid steppe, which extends onto the Patagonian plains to the east. During maximum glaciation, outlet glaciers draining the former Patagonian Ice Sheet and the alpine Cordillera Paine ice cap coalesced to form a single ice mass that extended eastward to deposit the Río de las Viscachas (RV) moraine systems at Torres del Paine. After local maximum glaciation, Torres del Paine glaciers separated to form three distinct ice lobes: Laguna Azul, Lago Sarmiento and Lago del Toro ice lobes and deposited the TDP I, II, III and TDP IV moraine belts (Marden and Clapperton, 1995; García *et al*., 2014; Fig. 1).

2. Methods

We selected six stratigraphic sites along El Canal sediment trench based on three main objectives: **1.** to include all major lithofacies associations (LFA); **2.** to record recurrent sediment sequences; and **3.** to mark key stratigraphic breaks. Based on qualitative and quantitative sedimentologic observations, such as sediment texture, color, degree of sorting, clast fabric, structures, and bed contact geometry, we divided stratigraphic sections into discrete lithofacies units. Our sedimentologic analysis included a panoramic approach (*e.g*., Evans *et al*., 2012) to define lateral stratigraphic relationships existing among the lithofacies. In order to obtain a complete picture of the morphostratigraphic record, we also connected the sediment sequences at El Canal with the surface morphology. By comparing the surficial morphology and underlying sediment record we correlated specific sediments units and sequences to landform building (*e.g*., moraines) and thereby defined glacial processes and environments at the ice front. Our method allowed us to define eight different LFA that comprise subglacial, subaquatic, and subaerial glacigenic sediments. We also sampled small pumice grains embedded within El Canal sediments for ICP-MS trace-element geochemical analysis both in order to identify provenance and to constrain the tephrochronologic context for sediments in El Canal by comparison with the products of dated eruptions from nearby volcanoes (Stern, 2008; Stern *et al*., 2011).

3. Results

In this section we first briefly describe the glacial landforms in the Torres del Paine region and then provide a detailed characterization of the sediments and tephra contained within El Canal site (Table 1 and 2; see García *et al*., 2014, for more details in the geomorphology).

3.1. Glacial landforms

Moraines in the Torres del Paine region include the inner TDP I, II, III, IV, and the outer RV belts (Marden and Clapperton, 1995; García *et al*., 2012; García *et al*., 2014). The TDP landforms at Lago del Toro and Lago Sarmiento are similar in terms of morphology, number, size, and geographic pattern of ridges (Fig. 1). The TDP I moraine belt consists of a tall (~20 m), broad (as much as one kilometer) composite landform. In contrast, each of the TDP II to TDP IV belts is made up of five to ten sharp (*e.g*., slope angle 20-30º), small (2-10 m high) and narrow (~5 m width) ridges (Marden, 1993; García *et al*., 2014). Glaciofluvial corridors commonly separate TDP moraines. The overall sinuosity of the moraine crests is punctuated by abrupt (*e.g*., 90º) changes in direction that define an indented geometry. The TDP IV landforms may be slightly higher in elevation than the outer TDP II and III ridges, resulting in the latter landforms being reworked and partially infilled by outwash sediments during TDP IV advance.

Only the inner TDP II, III and IV moraines are well-dated at present. Previous studies (Fogwill and Kubik, 2005; Moreno *et al*., 2009; García *et al*., 2012) indicate that these moraines date to the Antarctic Cold Reversal. Exposure dating applied to 38 boulders resting on these three landforms at Laguna Azul and Lago Sarmiento basins show that ^{10}Be mean ages for

TABLE 1. TRACE-ELEMENTS IN PUMICE GRAINS FROM LITHOFACIES ASSOCIATION D (PUMICE, PPM) COMPARED TO REPRESENTATIVE RECLUS (REP R1, 15,044±528 KA; STERN, 2008; STERN *ET AL*., 2011), R1 RANGE OBTAINED FROM ANALYSIS OF MULTIPLE SAMPLES, AND OTHER YOUNGER RECLUS TEPHRA.

	Pumice (ppm)	rep R1 (ppm)	R1 range (ppm)	Other R (ppm)
Ti	2,957	3,394	2,790-3,500	-
Mn	705	670	590-689	-
Cs	0.8	0.6	0.5-0.8	-
Rb	26	24	21-34	21-30
Sr	486	548	413-560	468-527
Ba	398	340	317-467	398-418
Y	11	10	sep-14	sep-13
Zr	107	103	71-144	109-161
Nb	13	11	sep-13	08-dic
Hf	1.5	1.8	1.1-2.1	1.3-1.8
Th	3.9	4.1	3.2-4.4	-
Pb	7.8	6.9	5.6-7.5	-
U	0.8	0.8	0.7-1.1	-
La	18.4	18.6	16.6-21.5	20.5-21.0
Ce	38.1	38.5	32.9-41.2	-
Pr	4.22	3.87	3.5-5.4	-
Nd	15.7	15.8	13.9-19.9	-
Sm	3.28	3.41	2.9-4.0	-
Eu	1.11	1.02	1.02-1.19	-
Gd	3.40	3.06	3.0-4.4	-
Tb	0.42	0.40	3.6-4.8	-
Dy	2.19	1.98	1.8-2.4	-
Ho	0.45	0.36	0.3-0.5	-
Er	1.30	1.10	1.0-1.4	-
Tm	0.17	0.11	0.1-0.2	-
Yb	1.24	0.99	0.9-1.3	1.0-1.24
Lu	0.19	0.11	0.1-0.2	-

each moraine belt are indistinguishable at 1 sigma and that all three belts were deposited at 14,150±560 ka (García *et al*., 2012). Deglaciation from the TDP IV moraines was underway by about 12,500 ka.

Because of mountainous relief, glaciofluvial plains at some locations were deposited in narrow corridors between the former ice snout and bedrock topography. El Canal spillway starts at the present Lago del Toro shoreline, proximal to the inner TDP IV moraine, and crosses all of the TDP I to IV ridges. The natural channel is ~2.5 km long and as much as 750 m wide. The channel was a main meltwater drainage route during and particularly after deposition of the TDP II-IV moraines. Four to five unpaired outwash terraces are inset along the channel and are particularly well developed on the northeastern bank between the TDP II and TDP I belts (Fig. 2 II).

TABLE 2. SEDIMENT LITHOFACIES ATTRIBUTES INTERPRETED FROM THE EL CANAL STRATIGRAPHIC SECTION (CODES FROM EYLES *ET AL*., 1983).

Lithofacies Association	Lithofacies	Code	Sedimentary structures
A shallow lake environment	sand, silt	Fl	fine lamination, very small ripples
	silt, may include scatter coarse sand	Fm	massive to very fine lamination
	sand, silt	Sl	low angle (10º) crossbeds
	sand	Sr	ripple marks
B ice-distal lake environment	silt	Fm	massive to very fine lamination
	sand, silt	Fl	fine lamination, very small ripples
	silt with dropstones	F-d	laminated or massive
	sand	Sh	horizontal lamination
C ice-proximal lake environement	silt with dropstones	F-d	laminated or massive
	sand, silt	Fl	fine lamination, very small ripples
	fine sand, silt	Fls	fine lamination sheared and deformed
	silt and gravel, including cobble	Dmm	diamictic massive
	silt and gravel, including cobble	Dms	diamictic stratified
D grounding line subaqueous fan	sand, silt	Fl	fine lamination, very small ripples
	sand	Sr	ripple marks
	sand, silt	Sl	low angle (10º) crossbeds
	gravel	Gt	trough crossbeds
	gravel	Gp	planar crossbeds
	gravel	Gh	horizontal bedding
E ice-contact slope	silt and gravel, including boulder	Dms	diamictic matrix supported stratified
	silt and gravel, including boulder	Dcs	diamictic clast supported stratified
	silt and gravel, including boulder	D--s	diamictic sheared, thrusted
F distal moraine slope	silt, sand, gravel	Gm	crudelly bedded
	silt, sand, gravel	Gp	planar crossbeds
	silt, sand, gravel	Dms	diamictic matrix supported stratified
G glacier bed	silt and gravel, including cobble	Dmm	diamictic matrix supported massive
H outwash plain	sand and gravel	Gm	crudelly bedded gravel
	sand and gravel	Gh	horizontal bedding
	sand and gravel, including cobble	Dmm	diamictic matrix supported massive
	sand and gravel, including cobble	Dcm	diamictic clast supported massive

3.2. Glacial sediments

We separated sediments at El Canal into eight LFA (*i.e*., A-H), each including one or more sediment lithofacies (Table 2; Figs. 2-4). Lithofacies codes and interpretations are based on and modified from Eyles *et al*. (1983).

3.2.1. Lithofacies Association A (facies codes: Fl, Fm, Sl, Sr)

This LFA consists mostly of sandy silt ripple beds, with occasional massive to faintly laminated fine sand and silt with sparse fine gravel. Ripples display a variety of geometries, internal structures, and, to some degree, grain size. They are mostly symmetrical. Silt appears mainly as tangential and concave-up foreset laminae and as horizontal undulating laminae outlining the geometry of the underlying ripples (*e.g*., draped lamination; Fig. 2 III and V). Fine sand laminae are deposited mainly as tangential and abrupt foresets, although horizontally laminated sandy beds occur interbedded with climbing ripples (Type B). Overall, internal ripple structure consists of foreset laminae dipping in either a single or opposite direction of flow (up and down-ice direction), chevron structures (mostly sandy silt ripples) and climbing ripple-cross lamination. Convoluted ripple beds usually occur underlying a massive to faintly laminated silt. The contact between these two units is conformable (Fig. 2 III).

Interpretation: shallow lake environment. This LFA was formed in a glaciolacustrine or ponded glaciofluvial environment. Although symmetric ripples resemble deposition by wave action, weak cross-sectional asymmetry was likely produced by mass transport in the direction of wave and overall current propagation in shallow waters. Chevron structures are indicative of wave action in a shallow-water environment. Climbing ripples formed from bottom traction combined with settling from the water column associated with overflows (Reineck and Singh, 1980). The existence of concave and tangential foresets in the internal structure of ripple marks also denotes extensive sedimentation from the water column (Jopling, 1965). Therefore, the sequence displays alternation between times when traction along the bottom is dominant and times when settling from the water column dominates (pure silt beds).

3.2.2. Lithofacies Association B (facies codes: Fm, Fl, F-d, Sh)

This LFA, which may be several meters thick, contains mostly pure silt forming plane beds, which occasionally appear interbedded with distinct gravel-rich silt layers reaching a few millimeters to centimeters thick. Lamination is very fine, horizontal and parallel (Fig. 2 VI) but can expose occasional wavy geometries (Fig. 2 IV). In the latter, interlayered sand and silt occur. Gravel bands are conformable on both the lower and upper boundaries. Occasional coarse clasts deform both the overlying and underlying fine sediment laminae (Fig. 3 II). Some silts conformably grade to well-laminated fine sands. The bedding contact with the overlying unit is commonly sharp and unconformable (Fig. 2 I, 3 I).

Interpretation: ice-distal lake environment. This LFA represents glaciolacustrine sediments settled mostly from suspension (Benn, 1996; Johnsen and Brennand, 2006). Wavy and sandy silt ripple beds formed by traction associated with lake-bottom flow (Gustavson, 1975), which also produced the horizontally laminated sand. Nevertheless, the sediment is mostly pure silt, which likely originated as a blend of draped lamination and gentle bottom currents in a high sedimentation-rate distal glaciolacustrine environment (Gustavson, 1975; Ashley, 1975). Gravel-rich silt layers may have originated as ice-rafted debris and/or as moving clasts transferred from abrupt slopes at the ice margin (Benn, 1996).

3.2.3. Lithofacies Association C (facies codes: F-d, Fl, Fl(s), Dms, Dmm)

This stratified diamict is made up of interbedded silt, fine sand and coarser material (typically close to pebbly grain size and occasionally reaching cobble size; Fig. 3 I and II). Interlayered deformed silt and fine sand are conspicuous. Both irregular and asymmetric folding is common. Where stratigraphically associated with LFA-D, the sediment exposes shearing and folding structures. Coarse sediment occurs as poorly sorted, matrix-supported gravel layers (several millimeters to centimeter across). Clasts are subangular to subrounded. There is recurrent variation between fine (silt) and coarse (gravel) end members (Fig. 3 I and II), which provides the distinctive stratification of this LFA. Careful analysis of platy pebbles can reveal a moderate clast fabric oriented downstream (to the east). Cobbles, where present, deform both

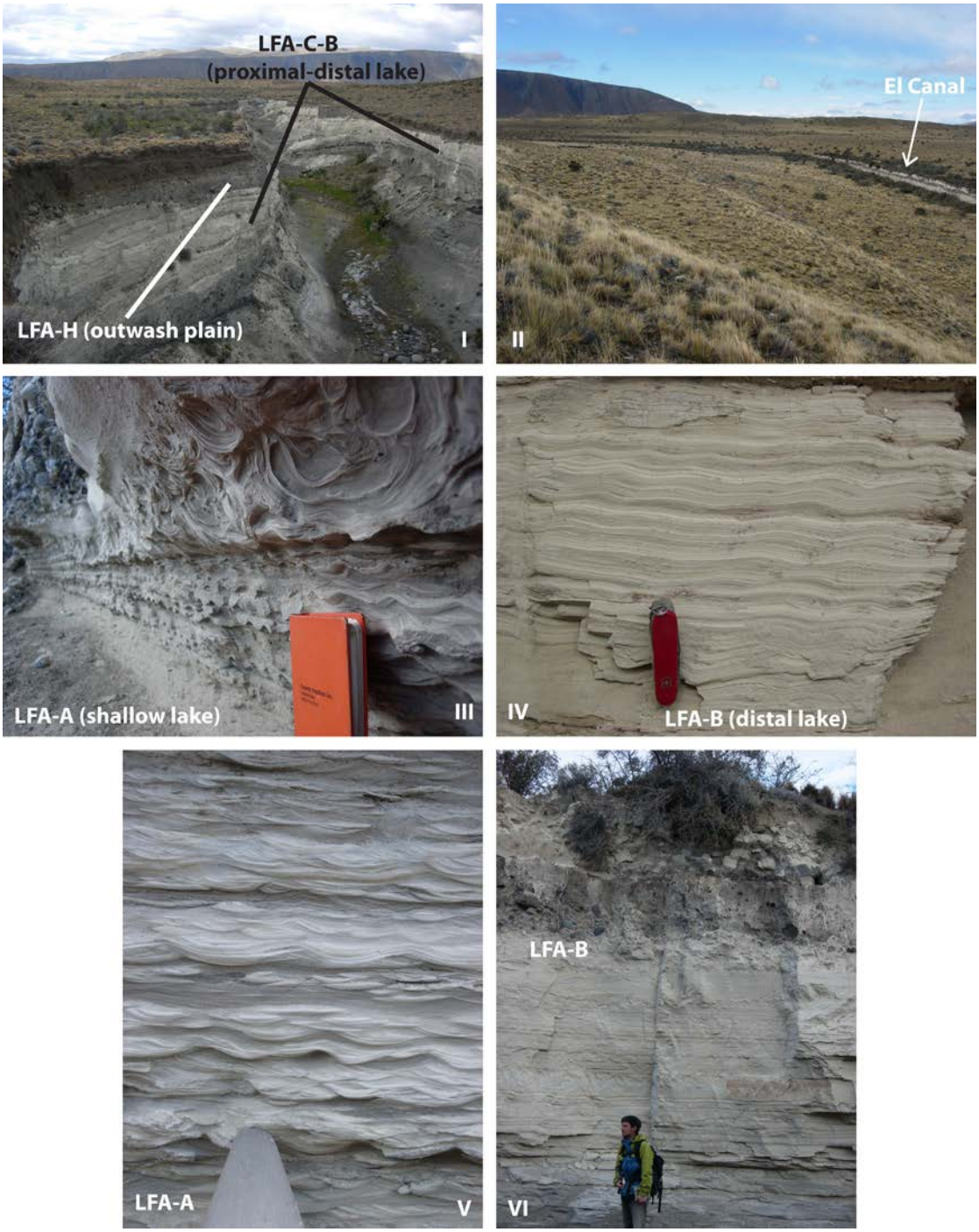

FIG. 2. Sediment lithofacies associations (LFA) in El Canal stratigraphic section. **I.** El Canal meltwater channel and stratigraphic section; the photo shows subaerial outwash deposits overlying glaciolacustrine sediments (view towards the SEE); **II.** foreground: distinct erosional terraces linked to the El Canal meltwater channel (arrow points to the El Canal sediment section, view towards the SE); **III.** sediments of LFA-A including deformed soft-sediment overlain by faintly laminated silt including sporadic tiny gravel near stratigraphic section i. Note overlying LFA-H sediments in the background; **IV.** wavy sediments of LFA-B; **V.** silty sand ripples from LFA-A near stratigraphic section i; **VI.** Faint to well laminated silt of LFA-B.

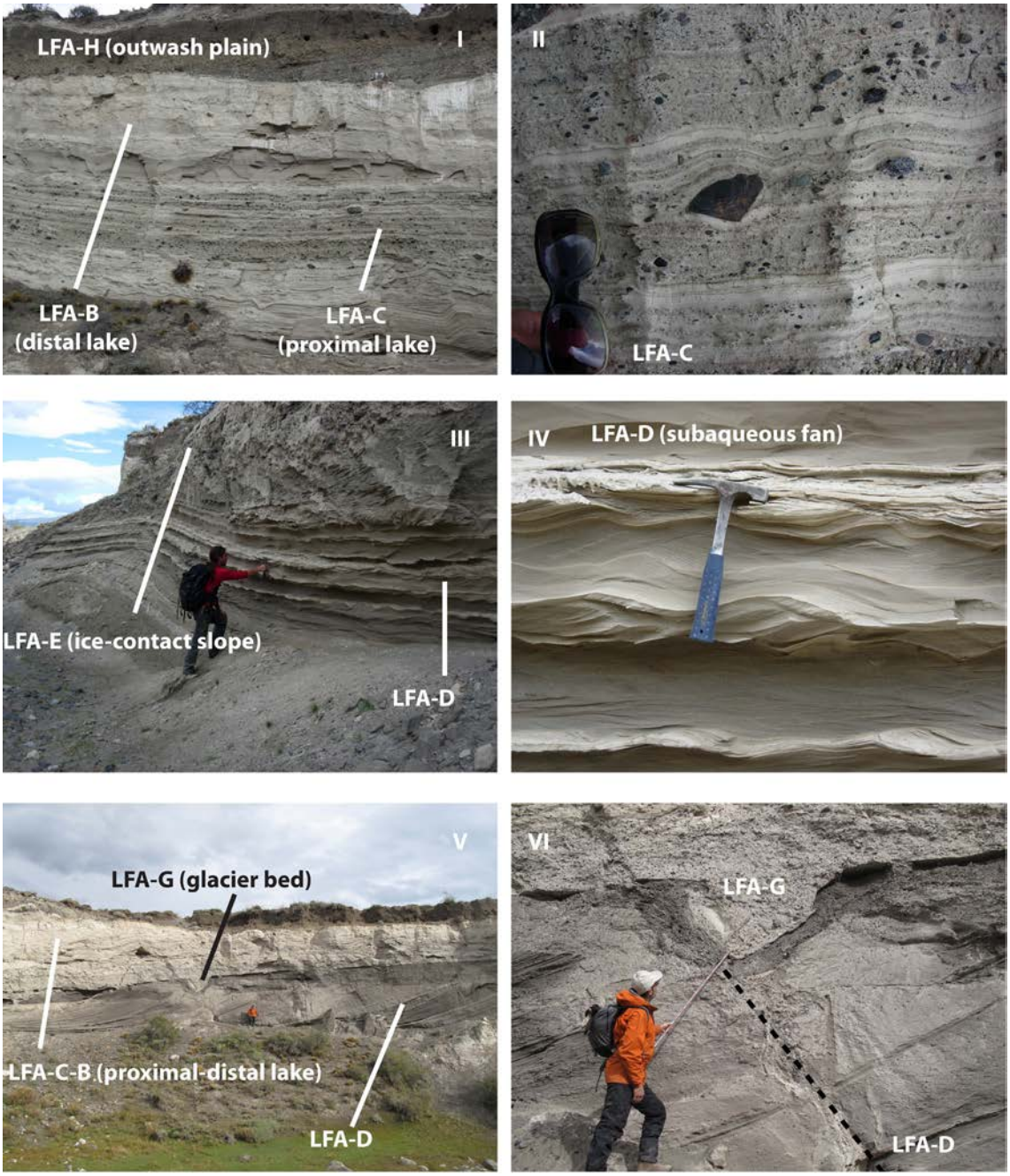

FIG. 3. Sediment lithofacies associations (LFA) in El Canal stratigraphic section. **I.** interbedded silt and gravel of LFA-C, overlain by silt of LFA-B and then by outwash gravel of LFA-H; **II.** Detail of LFA-C sediments in I. Note on-lap lamination on main clasts but absence of significant disturbance on underlying sediment layers; **III.** distal subaqueous fan sediments of LFA-D overlain by LFA-E sediments just west of stratigraphic section ii; **IV.** detail of LFA-D sediments at III. Note the rhythmic fashion between sand and silt beds; **V.** gravelly sand foresets of LFA-D unconformably overlain by till of LFA-G and glaciolacustrine fine sediments (LFA-B and C) at and just west of the stratigraphic section iv; **VI.** erosional contact between LFA-D and G at stratigraphic section IV. Note the ice-keel turbate and the sediment dike (black dashed line) intruding the sediment sandy unit.

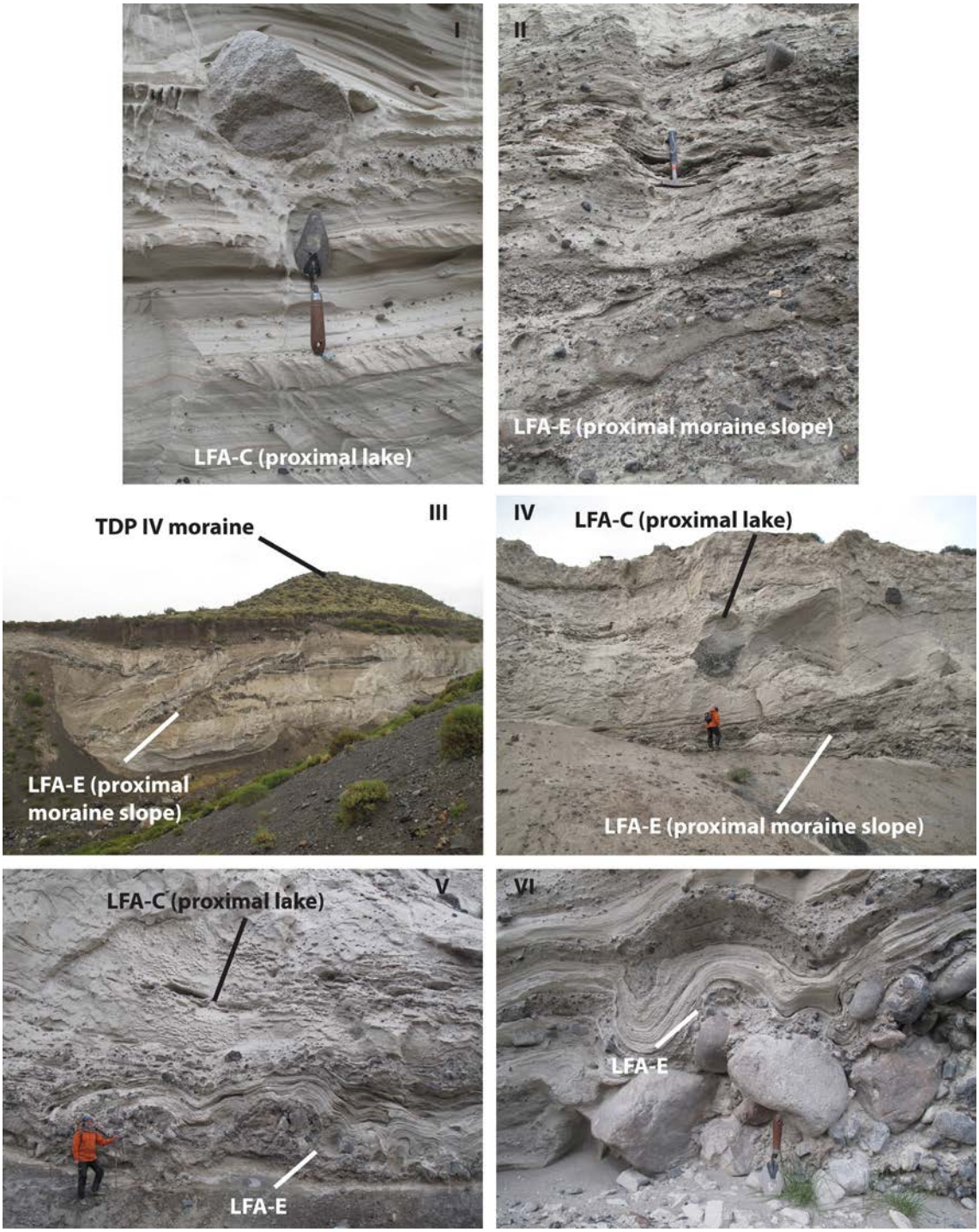

FIG. 4. Sediment facies associations (LFA) in El Canal stratigraphic section. **I.** composite sediment of LFA-C, including interlayered ice rafted debris (IRD), traction gravels and draped silt; **II.** Deformed proximal subaqueous outwash and mass flow deposits of LFA-E; **III.** Stratigraphic section vi with the TDP IV moraine ridge at the surface of the site (section is about 7 m high); **IV.** Glaciolacustrine sediments, including IRD (note big dropstone at the center of the photograph), overlying diamictons of LFA-E, west of stratigraphic section vi; **V-VI.** folded gravel beds of LFA-E, west of stratigraphic section vi (spatula is about 30 cm).

the underlying and overlying silt laminae, which is not commonly the case with the smaller grain size clasts. Conical shaped sediment mounds made up by coarse gravel occur surrounded by fine, well-laminated silt. Disturbance of underlying beds is insignificant, but overlying laminae generally onlap these conical mounds (*e.g.*, Thomas and Connell, 1985).

Interpretation: ice-proximal lake environment. This LFA resembles subaqueous sediment deposited distal to the ice margin under high sedimentation rate conditions (Gustavson, 1975; Ashley, 1975) and where bottom transport and settling from the water column coexist (Benn and Evans, 2010). Gravelly diamicton layers may have originated by more than one process. Cobble-sized clasts with distinct deformation of adjacent silt laminae are dropstones from icebergs (Fig. 4 I and IV). Symmetric, conic-shaped diamict mounds within well-laminated silt most likely correspond to icebergs dump deposits (Thomas and Connell, 1985). This suggests that icebergs were present and much of the diamicton may have originated as ice-rafted debris (IRD). Gravel layers can be followed laterally for several meters (Fig. 3 I), similar to well-stratified sediments described elsewhere as undermelt diamictons (Gravernor *et al*., 1984). Well-developed stratification can be the result of temporal (*e.g.*, seasonal) changes of environmental conditions producing the rhythmic gravel-silt sequence. In addition, gravelly diamicton layers could reflect other subaquatic processes (Benn and Evans, 2010), such as distal debris flows and fall, traction currents along the lake bottom (*e.g.*, suggested by moderate clast fabric), or settling from suspended plumes. Fine sediment folding is related to proglacial deformation associated to a nearby ice front fluctuation. In summary, the diamict units in this LFA reflect a relatively proximal glaciolacustrine environment, affected by a high concentration of icebergs and traction currents delivering coarse sediments to the site.

3.2.4. Lithofacies Association D (facies codes: Fl, Sr, Sl, Gt, Gp, Gh)

This LFA includes mostly gravel and sand, but silt is also present. Gravel occurs mainly as gravel sheets and clinoforms; sand and silty sand tends to form cross bedded to faintly laminated sediment units, commonly exposing undulating and rhythmic laminations (Fig. 3 III-VI). Sandy gravel clinoforms grade to finer cross-laminated sand and silt forming horizontal, parallel beds. In some sections, both sediment types overlap, separated by erosional surfaces. There is an overall distal decrease in grain size. Fine sand ripple-cross lamination (*e.g.*, in drift; McKee, 1965) appears rhythmically interbedded with draped silt beds (Fig. 3 III and IV). Sand cross lamination includes eroded (*i.e.*, type A ripples) and aggrading stoss side climbing ripples (*i.e.*, type B ripples), with the latter displaying high angles of climbing (Fig. 3 IV). Draped silt beds are very distinct and continuous and provide an undulating appearance. Ripples foresets vary from straight to concave up lamination and show an eastward (down-ice) flow direction. Overall, the finer sediments of this LFA display cosets of draped silt beds (sinusoidal lamination; Johansen and Brennand, 2006) overlying type B ripple-drift, which in turn overlies type A ripple cross lamination, a sequence that rhythmically repeats within the outcrop. Reverse faulting can occur within sandy silt laminated sediment.

Small (<3 mm) pumice grains are widespread in LFA-D. Trace-element geochemical analysis of these grains indicate that they are similar to pumice and bulk tephra derived from explosive eruptions of the Reclus volcano (Table 1; Stern 1990, 2004 and 2008), the nearest volcano in the region located ~30 km west of Torres del Paine and ~75 km west of the El Canal section.

Interpretation: Grounding-line subaqueous fan. The sediment structure, grain size, and geometry of units suggest bedload transport and deposition on a prograding subaqueous slope (Benn, 1996). The sequence displays downstream fining, which is typical for grounding-line subaqueous fans (Benn and Evans, 2010). The sandy gravel clinoforms represent slip faces (Boothroyd and Ashley, 1975) caused by avalanching of sediments. Ripple sand cross lamination distal to the foresets denotes a decrease in flow strength, (Johnsen and Brennand, 2006; Evans *et al*., 2012), likely related with turbulent underflows (Benn, 1996). Rhythmic variation of sediments grading from ripple type A-drift to type B-drift climbing cross lamination and then to draped lamination reflects a decrease in current strength and an increase in the ratio of suspended to bedload sediment (*e.g.*, Gustavson, 1975; Reineck and Singh, 1980). These sediments are likely associated with underflows (Benn, 1996) and/or fluctuations of the sediment input from meltwater conduits into a glaciolacustrine system.

3.2.5. Lithofacies Association E (facies codes: Dms, Dcs, D--s)

This LFA is poorly sorted deformed gravelly silt interbedded with overthrusted diamict (Fig. 4 II). Gravelly silt can be massive or layered with folded silty sand. Sediment beds dip as much as 10º above the horizontal. Surface contacts are irregular and sharp. Clasts, including mostly pebbles and cobbles, are subangular to subrounded (Fig. 4). Outsized clasts are common. Some clasts are well faceted and include striations. The facies displays sheared sediments that can display symmetric, overturned and polyclinal folding (Fig. 4 V and VI). Dislocated irregular gravel lenses embedded in fine sediments also occur.

Interpretation: ice-contact slope. This LFA includes proximal grounding-line outwash and debris flows that have been glaciotectonized by compressive pushing and grounding of ice. Based on the presence of moraine ridges on the land-surface above these sediments, we associate this LFA with moraine construction (Fig. 4 III). The glacier snout built the moraine ridges by shortening and uplifting deformable saturated glaciolacustrine sediment, including those originated from gravity process (*e.g.*, subaqueous sediment gravity flows, mass wasting deposits) and meltwater entering a lake at the ice margin.

3.2.6. Lithofacies Association F (facies codes: Gm, Gp, Dms)

This LFA consists of crudely cross-bedded diamicton arranged as parallel, matrix- supported coarse gravel clinoforms interfingered with well-laminated silts and gravelly sand. Gravel beds are several decimeters thick and dip eastwards (downstream) as much as 15º. Sandy gravel and silt units that interrupt the diamict make up crude bedding. Clasts are mostly subangular and are commonly smaller than cobble size, but are as large as boulders. Grain size tends to become coarser downslope in the gravel beds.

Interpretation: distal moraine slope. Based on the stratigraphic context, sediment architecture, structure, and sorting, we interpret this LFA as being deposited by debris flows as an ice-contact fan. The coarse gravel clinoforms form a prograding slope. The poor sorting and the conformable relationship with underlying diamicton (LFA-G) indicate deposition as from the ice margin (Benn and Evans, 2010). Conformable lower contacts indicate non-erosional and unchannelized flows (Benn, 1996). Interbedded well-laminated sandy gravel and silt suggest that this LFA includes stacked debris flows and sediment-loaded meltwaters entering a glacial lake.

3.2.7. Lithofacies Association G (facies codes: Dmm)

This LFA consists of massive gravel diamicton with high variability in the clast to matrix ratio and clast size. For instance, gravel may be abundant or dispersed, floating in an indurated silt matrix (Fig. 3 V and VI). Clasts are subrounded and subangular, may have well-developed facets, and are as large as cobble size. Sediment is mostly structureless. Massive diamicton is interrupted by well-laminated, deformed fine sediment in places.

Interpretation: Glacier bed. The massive to coarsely bedded aspect of this coarse gravel LFA, together with its sediment structures and faceted clasts, suggest ice-proximal debris-flow deposits that have been homogenized in the subglacial position (*e.g.*, Boulton, 1987; Benn, 1996; Benn and Evans, 2010). Sedimentary dikes and deformed stratified sediments of the underlying unit indicate loading pressure imposed by overriding ice.

3.2.8. Lithofacies Association H (facies codes: Gm, Gh, Dmm, Dcm)

Overall, well-sorted sandy gravel makes up horizontal beds that in places can be traced laterally for tens of meters (Figs. 2 I, 3 I). Bedding commonly is rudimentary or absent. An apparent moderate fabric indicating eastward direction of flow is present. Clasts are rounded to subangular and commonly pebble-sized, although clasts as large as cobbles are present, particularly close to moraine slopes. Although generally moderately sorted and clast-supported, this sediment varies significantly along a west-east transect. Well-sorted fine gravel packages may be included within poorly sorted coarse gravel. The sediment forms a tabular-shaped unit with an unconformable planar contact, but it displays channel-cut erosional surfaces also. Sediment of this LFA, where present, occurs at the top of the El Canal stratigraphic sequence.

Interpretation: outwash plain. The massive to coarse bedding and limited sediment structures of this LFA likely resulted from rapid deposition close to the ice margin (Fahnestock, 1963; Church and Gilbert, 1975). Presence of units with better sorting and horizontal bedding may reflect greater distance from the ice margin and/or relatively low-energy flows.

A likely physical setting for deposition of this LFA is a channel-bar system in a proglacial braided river environment. This conclusion is based on similarity to other glaciofluvial records (*e.g.*, Clague, 1975; Marren, 2005), and on the fact that this LFA generally occurs at the top of the sediment sequence where it is exposed in cuts into the subaerial glaciofluvial plains and terraces. We interpret the tabular-shaped, poorly sorted sediment units with an unconformable planar contact, as colluvial sediment reworked by subaerial meltwater streams (Fig. 5).

3.3. Stratigraphic sections

We describe six stratigraphic sections distributed along El Canal from ice-distal to proximal sites (Fig. 1). Sections i, iii, iv and v occur on the southern side of El Canal trench, whereas ii and vi crop out on the north wall. Please refer to figures 5 to 10 for graphics of these sediment sequences that are described in order from lowermost to uppermost sediment units.

3.3.1. Section i (Fig. 5)

At the base of the section, grain size, ripple geometry (*e.g.*, symmetrical) and structure (*e.g.*, chevron structures) of LFA-A indicate wave action in a shallow lake. Overlying ripples and massive sandy silt can be linked to shallow-water lake currents. The convoluted ripples are genetically associated to the deposition of the uppermost LFA-H unit, a colluvium, as a consequence of post-depositional plastic deformation. Sediments removed during the artificial excavation of El Canal trench have been deposited on top of LFA-H and lack any geological significance (Fig. 5).

3.3.2. Section ii (Fig. 6)

Sandy ripples of LFA-D occur just few meters to the east of this sediment section (Figs. 3 III and IV, 6) and represent distal subaqueous fan sediments. Inverse and normal faults, widespread in the rippled sediments, together with overlying, deformed folded and overthrusted high-density underflow sediments of LFA-E, suggest ice loading and overriding the site. Both the coarsening of grain size upwards and the increase in the degree of sediment deformation between LFA-D and overlying LFA-E, demonstrate approaching and overriding ice. Both units are separated by an erosional unconformity. Based on the presence of LFA-E, this glacial advance may have ended with the formation of a TDP II moraine ridge. Such moraines occur nearby but not at the section, probably because of younger glaciofluvial erosion (*e.g.*, LFA-H outwash at the top of the section)(inset in Fig. 1). Westward retreat from this ice-marginal position enabled the site to be occupied with a glacial lake, as indicated by the fine-grained glaciolacustrine sediments of LFA-B. This lake extended eastwards at least to stratigraphic section i, where there is evidence for a shallow water environment. The subaerial glaciofluvial sediment that caps the section (LFA-H) was deposited during a later glacial stage.

3.3.3. Section iii (Fig. 7)

This stratigraphic section resembles the upper part of section ii, but is located few hundred meters in the up-ice direction. Gravelly silt layers from LFA-C cropping out at the base of the section indicate a glacial lake with icebergs depositing IRD with input from meltwater conduits (*e.g.*, Gravernor *et al*., 1984; Bennett *et al*., 2002). The decrease in grain size and absence of deformation within the overlying glaciolacustrine sediments of LFA-B suggest that ice had retreated further westward. As in stratigraphic section ii, the top gravel (LFA-H) was deposited by proglacial subaerial streams.

3.3.4. Section iv (Fig. 8)

The base of this sediment section (Fig. 8) shows gravelly sand crossbeds that distally grade to subhorizontal sandy ripple sets. The sediment bedding indicates eastward flow (down-ice direction) within a subaqueous fan (LFA-D). Clinoforms show the prograding fashion of these subaqueous sediment bodies (Benn, 1996). The gravelly fan sediments grade upwards unconformably to massive diamict sediments of LFA-G, suggesting glacier expansion over and beyond the site. Ice weight caused faulting and loading casts (Fig. 8). Till infills a conical depression that is shaped in the lower subaqueous fan deposits (Fig. 3 VI). Base on its shape and geological context, this depression most likely represents an iceberg keel scar in the lake bed (Thomas and Connell, 1985) or a local subglacial ice trough. As in stratigraphic sections ii and iii, the overlying LFA-C and B sequence, exposing a change into better-sorted and less deformed laminated silt, suggest glacier retreat to the west. Icebergs dump deposits (Thomas and Connell, 1985) occur within the laminated lake

FIG. 5. Stratigraphic section i. View is to the south. White arrow indicates ice flow direction.

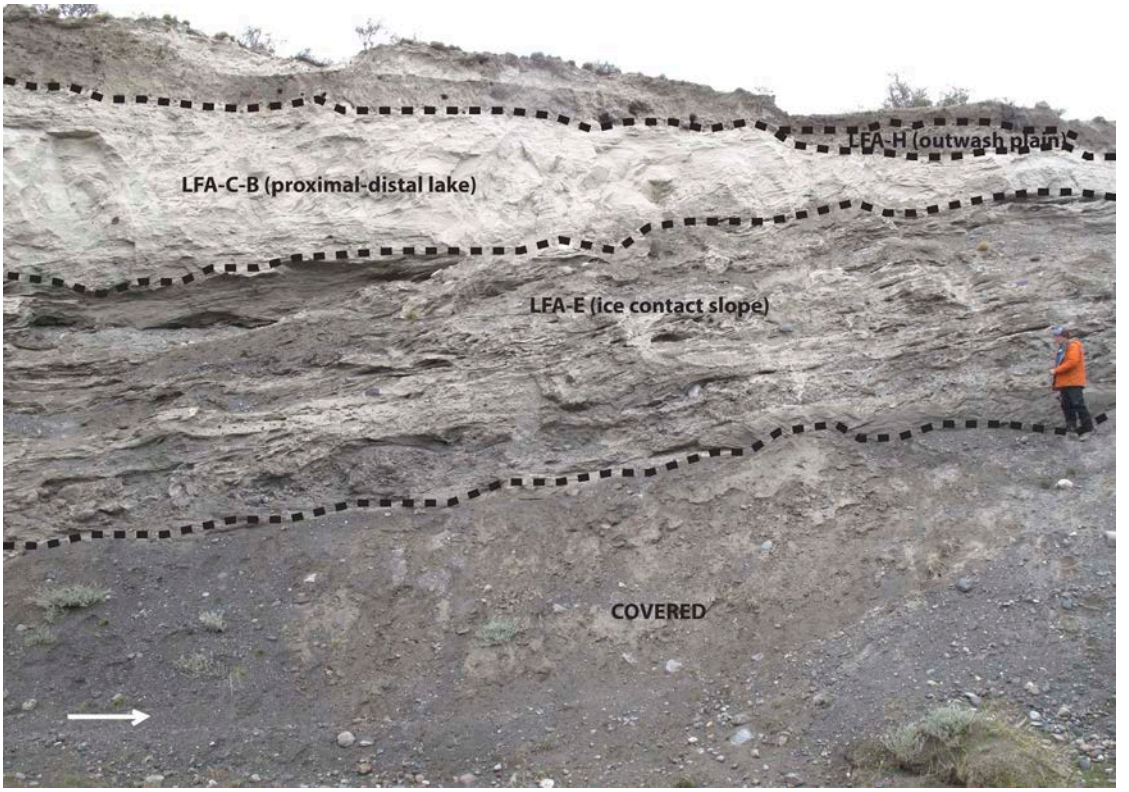

FIG. 6. Stratigraphic section ii. Lithofacies association LFA-D crops out at the base, just west of this section (Fig. 3 III, IV). View is to the north. White arrow indicates ice flow direction.

sediments. Proglacial glaciofluvial streams deposited the moderate to well-sorted, faintly stratified gravels of LFA-H at the top of the sequence.

3.3.5. Section v (Fig. 9)

A massive to coarsely stratified gravel diamicton occurs at the base of section v (Fig. 9) and resembles a subglacial deformation till described for LFA-G. The dipping beds overlying the subglacial till are typical of flow-tills (LFA-F) and most likely were deposited from the ice margin. This suggests that the ice front stabilized at stratigraphic section v for some time to build a moraine ramp. The interbedded gravels and silts of overlying LFA-F are consistent with the rudimentary normal grading that occurs with subaqueous debris flows. On top of the debris flows, a sediment unit including interbedded cross-laminated gravelly sand and silt ripples of LFA-D suggests that ice retreated from the site to build a proglacial subaqueous fan (Benn, 1996; Johnsen and Brennand, 2006; Evans *et al*., 2012). A massive till (LFA-G) was deposited uncomformably over the fan sediments, indicating ice overriding the site again. Disrupted gravelly sand and thrusting within LFA-D, unit resulted from ice pushing and overburden pressure on the subaqueous fan sediments. Whereas the western half of the sediment section is capped by the massive till unit of LFA-G, the eastern half displays the upper sediment sequence already described for stratigraphic sections ii, iii and iv: LFA-C, B and H sequence. These sediments denote glacial retreat from the site and, as a result, the development of a glacial lake occupied with icebergs, and later glaciofluvial subaerial streams.

3.3.6. Section vi (Fig. 10)

At the base, this sediment sequence shows a coarsely stratified to massive diamicton that we interpret as a subglacial deformation till (LFA-G). Overlying this unit, tangential gravelly sand crossbeds grade westwards (up-ice direction) to subhorizontal, silty sands, consistent with a subaqueous fan (LFA-D). Portions of this unit show fine, faintly

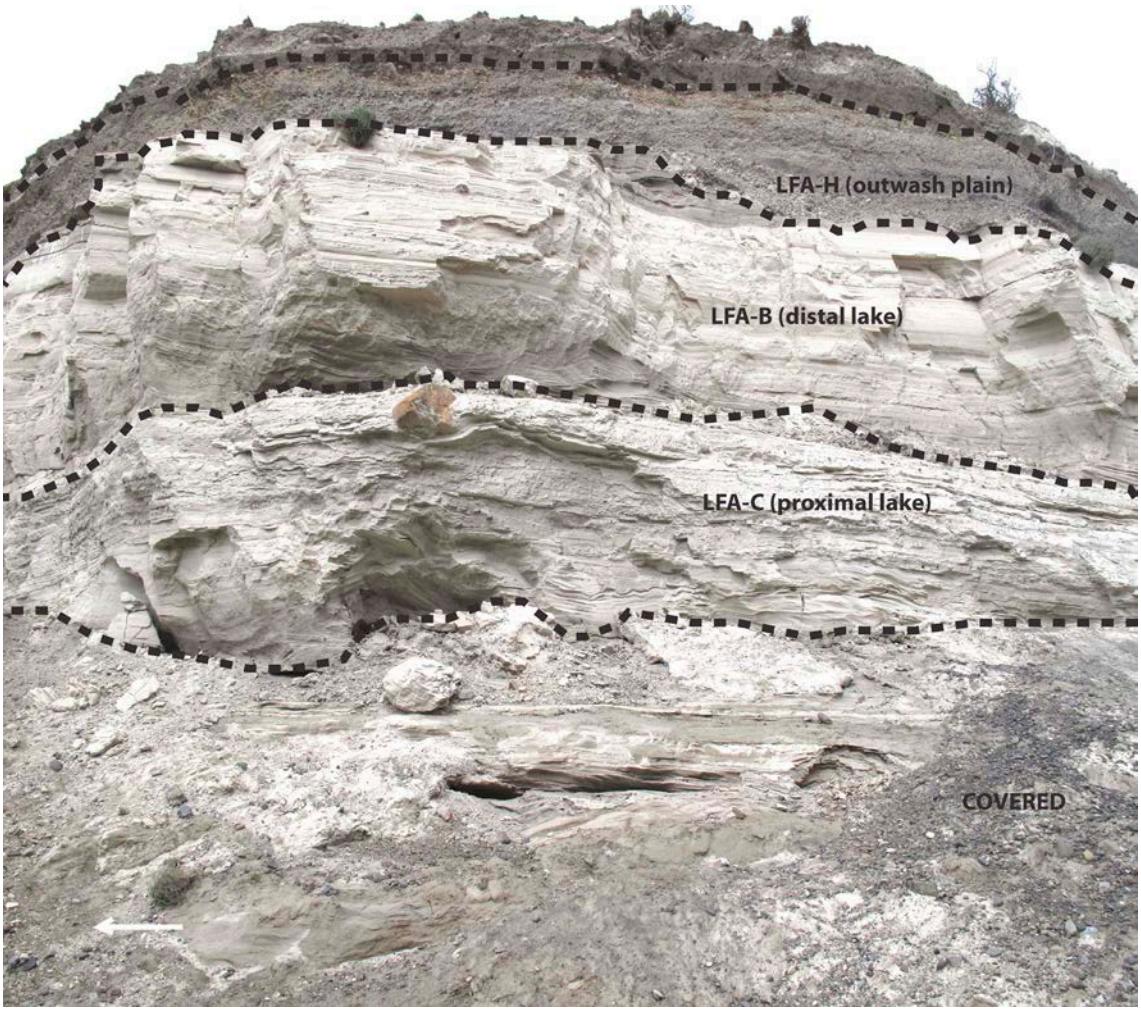

FIG. 7. Stratigraphic section iii. Section is about four meters tall. View is to the south. White arrow indicates ice flow direction.

bedded sediment (LFA-B; Fig. 10). A coarser, rippled gravelly sand (LFA-D) showing an eastward direction of flow overlies the westward flowing fan unit, which in turn is overlain by folded crudely stratified tilted gravels of LFA-E (Fig. 10). This sediment sequence is consistent with a glacial advance that built the subaqueous TDP IV moraine ridge on top of the section (Fig. 4 III). As in sediment section ii, glaciotectonized proglacial meltwater and debris-flow deposits make up the core of the moraine. Near the top of the section, the abundance of IRD embedded in well-laminated, locally folded silt (LFA-C) represents gradual glacial retreat from the site and the occurrence of a glacial lake occupied with icebergs. These glaciolacustrine sediments show the same trend as in the more distal sections described above: folded gravelly silts at the base and clean undeformed silt towards the upper part of the sequence (containing only sparse dropstones). The upper glaciofluvial gravels from LFA-H cap the sequence, indicating that the glacial lake eventually was filled with sediments and/or drained completely. Here, outsized boulders represent colluvial sediments reworked by meltwater streams.

4. Discussion and conclusions

The panoramic analysis of lithofacies (*e.g.*, Evans *et al.*, 2012) at six stratigraphic sections along El Canal trench allows us to reconstruct subaquatic

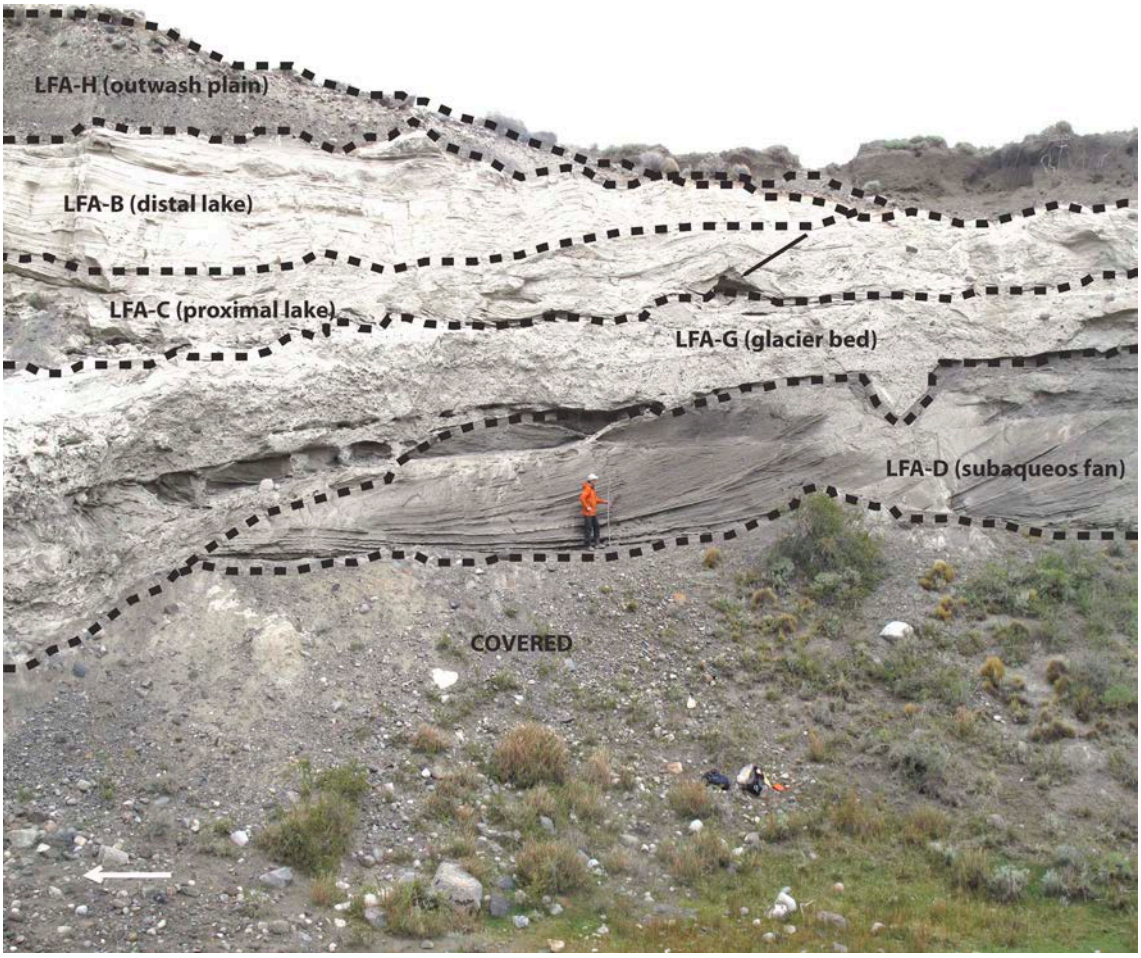

FIG. 8. Stratigraphic section iv. Black arrow points to iceberg dump deposits within lithofacies association C. View is to the south. White arrow indicates ice flow direction.

and subaerial glacial processes and environments. Figure 11 displays a reconstruction of late-glacial ice fluctuations and environments of Lago del Toro ice lobe.

4.1. Glaciolacustrine environments

The sedimentologic record at El Canal affords evidence for a glaciolacustrine system along the eastern Lago del Toro ice-marginal zone at the end of the last glaciation. The sedimentologic and morphologic evidence suggests that glacial lakes existed during deposition of the TDP II to IV moraine belts. Several pieces of evidence point to these lakes being local in extent (*e.g.*, contained by TDP moraine ridges), rather than the regional-scale lakes described before for Torres del Paine (Solari *et al*., 2012; García *et al*., 2014). For example, glaciolacustrine clay typical of deep glacial lakes in the region (Sagredo *et al*., 2011) is absent. The presence of chevron structures and symmetric ripples shaped by the wave action indicate shallow lake waters. Moreover, the presence of several meltwater channels, of which El Canal is by far the most prominent, suggests the existence of discrete lake systems at the front of the Lago del Toro ice lobe. Similarly, the presence of subaerial outwash gravel and glaciofluvial plains grading to the moraines suggests that lacustrine bodies eventually were infilled, which implies that they were relatively restricted water bodies. However, the lakes were extensive enough to allow differentiation between shallow and deep-water environments and

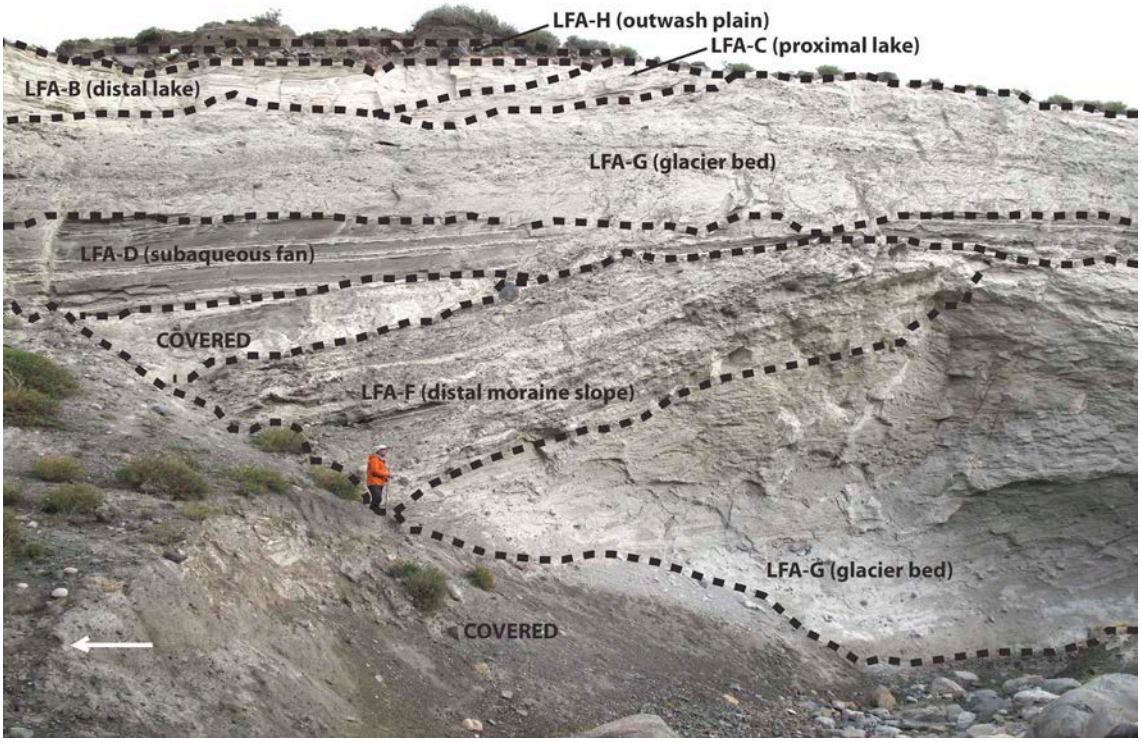

FIG. 9. Stratigraphic section v. View is to the south. White arrow indicates ice flow direction.

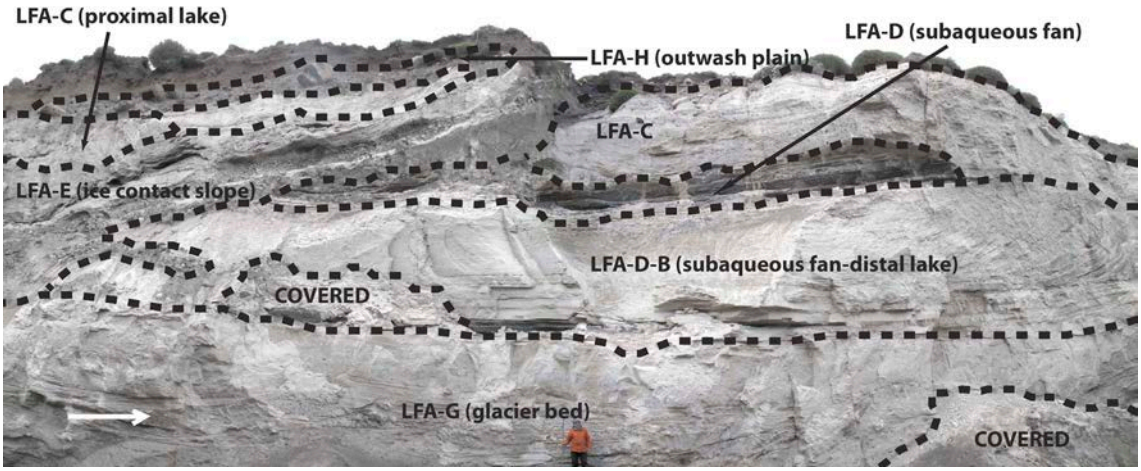

FIG. 10. Stratigraphic section vi. View is to the north. White arrow indicates ice flow direction.

proximal and distal zones in the sedimentation. For instance, El Canal site includes a subglacial zone (LFA-G) lying behind the grounding line; an ice-proximal zone, which includes the area contiguous to the grounding line associated with the construction of moraines (LFA-E and F) and grounding-line fans (LFA-D), typical at temperate glacial lakes (Benn and Evans, 2010); a transition zone, with abundant

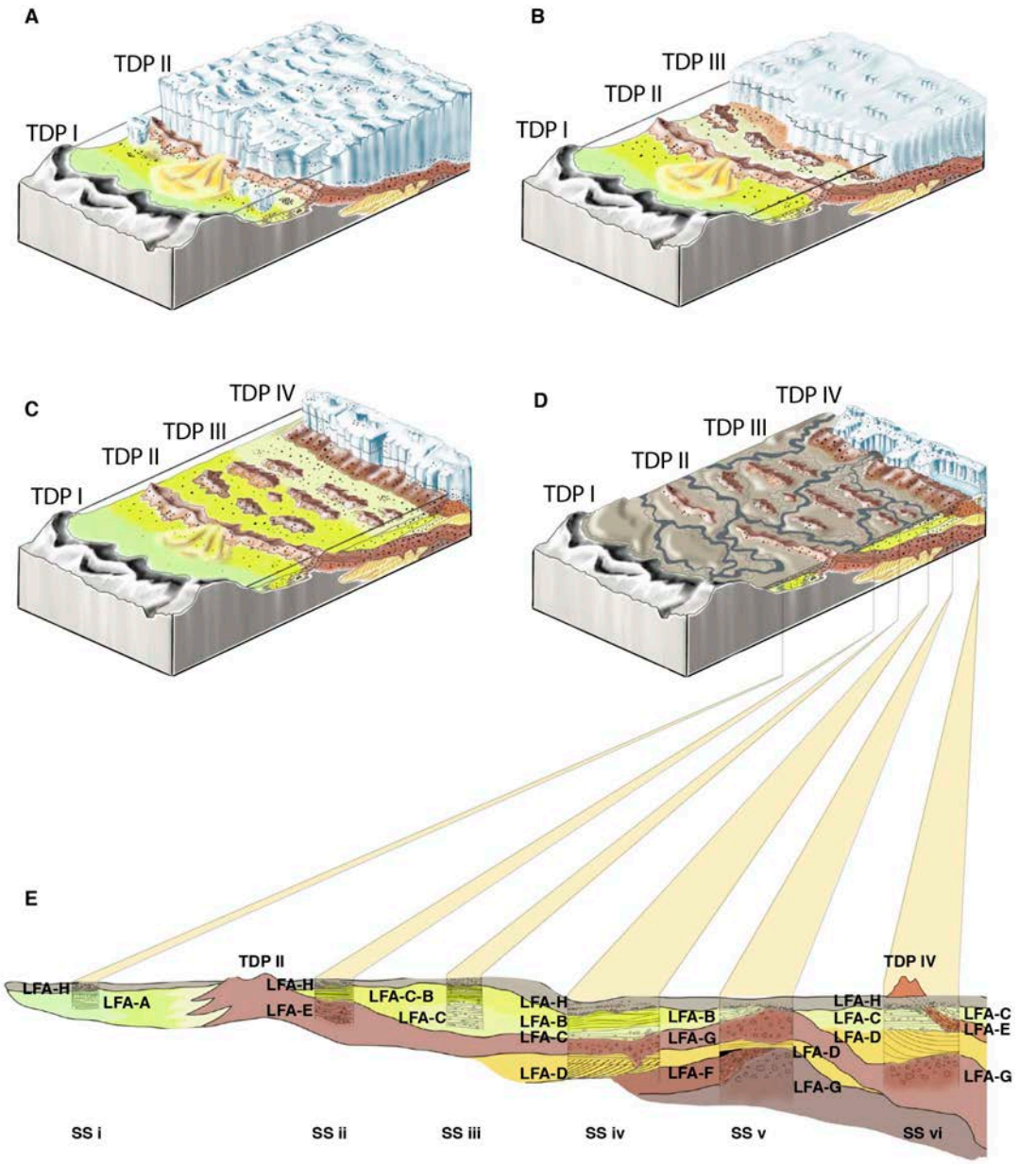

FIG. 11. Cartoon describing Lago del Toro ice lobe fluctuations as defined at the El Canal morphostratigraphic record. **A.** TDP II ice advance over a glacial lake; **B.** TDP II retreat and formation of glacial lake where previously occupied by ice. This stage includes the TDP III ice readvance inferred from the morphological record, but not preserved in the sediments; **C.** TDP IV readvance over a glacial lake; **D.** TDP IV retreat and complete subaerial conditions at El Canal Site; **E.** Zoom into the interpreted sediment record at El Canal stratigraphic section. **SS:** stratigraphic section; **LFA:** lithofacies association.

icebergs producing IRD reworked by traction currents to form layered dropstone diamictons (LFA-C); and a distal zone, dominated by drape silt lamination and scattered dropstones (LFA-B), which lacks major reworking of sediment.

The late-glacial lakes described here must have occurred after or during drainage of the large glacial paleolake Tehuelche (Solari *et al*., 2012; García *et al*., 2014) that occupied the Torres del Paine region during the last glacial period. In this scenario,

the prominent erosional shorelines at ~120 and 250 m a.s.l. at Sierra del Cazador (Fig. 1) are linked to a deeper and older glacial lake than to those water bodies interpreted from El Canal glaciolacustrine record.

4.2. Moraine building

Glaciotectonized and tilted debris flows deposits interbedded with proximal subaqueous outwash (*e.g.*, hyperconcentrated flows) relate to ice bulldozing and pushing during moraine building (Boulton, 1986; Benn, 1996). At sediment section ii, subaqueous fan sediments grade upward to deformed and overthrusted diamict stratified deposits originating at the ice front. The same type of sediment sequence occurs at section vi, where pervasive deformation of gravel beds embedded in fine glaciolacustrine sediments originated as the ice advanced to build the TDP IV moraine (Fig. 4 III). Therefore, our observations suggest that inner TDP II-IV end moraines formed from subaqueous push with active meltwater and mass-flow sedimentation along the glacier grounding line (Benn and Evans, 2010). In this model of moraine building, ice advanced and overrode ice proximal composite glaciolacustrine sediments. Ice bulldozing and pushing produced ductile and brittle deformation of sediments, the first being the most characteristic throughout the exposure. Glaciotectonic deformation was facilitated by high pore-water pressure of fine lake sediment prompted by impermeable underlying sediments (till) and bedrock lying close to the surface assuring low hydraulic transmissibility. Therefore, each ice advance by the Lago del Toro and Lago Sarmiento ice lobes compressed, tilted and uplifted proglacial sediment to produce the TDP II-IV moraine ridges. The characteristic sinuous and indented shape, sometimes exposing a characteristic saw-tooth pattern shape of these moraines (Lago Sarmiento ice lobe, Marden, 1993) provides the morphologic evidence for ice bulldozing and pushing of subaquatic sediments (Matthews *et al*., 1979). A particular aspect of TDP moraines is that they formed at shallow lake environments where grounding line sediment output was abundant (cf., McCabe *et al*., 1984; Eyles and McCabe, 1989; Benn, 1996). Rapid and abundant sedimentation caused these water bodies to be infilled and thus the moraines to become subaerial during the glacial advance, as reflected by outwash plains grading to the moraines. In fact, some of the TDP III and II ridges appear almost completely buried by outwash, exposing the accretion trend at this ice marginal setting.

4.3. Glacial fluctuations

Lithofacies associations E, F, and G at El Canal stratigraphic section document evidence for three distinct glacial expansions: TDP II, TDP IV and an older undefined glacial pulse identified at sediment section v. Whereas LFA-G indicates ice advancing over a site (*e.g.*, sediment sections iv, v and vi), LFA-E and F denote the culmination of an ice advance, linked to moraine building (sediment sections ii, v, vi; Fig. 4). Stratigraphic section ii displays a complete sediment sequence that shows the glacier advance that culminated with the construction of a TDP II ridge. Similarly, the stratigraphic transition from subglacial deformation till (LFA-G) to flow till sediments (LFA-F) at section v suggest the existence of a glacial advance preserved only within the El Canal sediment record. Presumably, this event was linked to a still-stand of the Lago del Toro ice lobe during retreat from TDP I ice marginal position, before TDP II readvance.

Panoramic (*i.e.*, lateral) stratigraphic relationships of sediment units between sections v and ii along El Canal trench expose the sedimentary evidence for the TDP II glacier advance and retreat. At sections v and iv the sequence reveals grounding-line subaqueous fan-sediments (LFA-D) overlain by massive glacial diamicton (LFA-G), which indicates (TDP II) ice approaching and overriding the sites. At section ii subaqueous fan deposits grade unconformably to tilted proglacial deformed sediments of LFA-E, which correspond well with the occurrence of a TDP II moraine ridge nearby. Glaciolacustrine laminated sediments that overlie diamict LFA-E and G in sections ii-v, can be tracked westward and indicate glacier retreat from TDP II ice marginal position, which was accompanied by the formation of a shallow glacial lake on the recently deglaciated area.

Whereas accretional processes dominated during the deposition of the TDP II-IV moraines, vertical and horizontal erosion characterized the retreat from TDP IV moraine belt. In this sense, ice-contact moraine building and proglacial glaciolacustrine sediment accumulation characterized each ice advance. After retreat from TDP IV moraines an

ice contact lake continue to exist which eventually merge as one whole lake in front of the glacier draining through the El Canal spillway. This stage lasted until a new spillway opened through Río Serrano, on the western margin of Lago del Toro, and El Canal channel was abandoned.

4.4. Geochronological implications

Although the chemistry of tephra in the Torres del Paine area produced by various late-glacial and Holocene eruptions of Reclus volcano are all similar (Stern, 1990, 2008), the only eruption older than the TDP II-IV moraines (14,150±560 ka; García *et al*., 2012) and coeval with El Canal sediments is the large late-glacial R1 eruption dated as 15,044±528 ka (Stern, 2008; Stern *et al*., 2011). Although no isopleth maps of maximum pumice dimensions have been obtained for this eruption, the small size of pumice grains at El Canal are consistent with their being derived from airfall deposits reworked by late-glacial TDP II, III and IV advances. In contrast, very large (>14 cm) pumice clasts found farther to the west in glacial and glaciofluvial sediments in the valley of Río Grey, were likely derived from the same R1 eruption, but were transported supraglacially, and deposited during glacial retreat after 12,500 ka (Stern, 1990, 2008; Marden and Clapperton, 1995). We therefore believe that our tephra analysis indicates another source of evidence showing that both the TDP II, III and IV landforms and sediments at Lago del Toro are late-glacial in age, most likely deposited during the Antarctic Cold Reversal chronozone, as the other TDP II-IV landforms in the area (*e.g*., Lago Sarmiento and Laguna Azul ice lobes).

Acknowledgements

This work resulted thanks to the support of the FONDECYT Iniciación #11110381 project and the Churchill Exploration Fund. We are very grateful to D. Belknap from University of Maine and M. Kaplan from LDEO for their valuable comments along this work. We also thanks to G. Gómez and J.J. Ferrada from the Pontificia Universidad Católica de Chile for assistance in the field and construction of figure 1. The Corporación Nacional Forestal (CONAF) Magallanes, Parque Nacional Torres del Paine (Chile) administration, and H. Cárdenas (Estancia San Antonio) were of great field support upon this research.

References

Ashley, G.M. 1975. Rhythmic sedimentation in glacial Lake Hitchcock, Massachusetts-Connecticut. *In* Glaciofluvial and Glaciolacustrine sedimentation (Jopling, A.V.; McDonald, B.C.; editors). Society of Economic Paleontologists and Mineralogists, Special Publication 23: 304-320. Tulsa.

Bentley, M. 1996. The role of lakes in moraine formation, Chilean lake district. Earth surface processes and landforms 21: 493-507.

Bennett, M.R.; Huddart, D.; Thomas, G.S.P. 2002. Facies architecture within a regional glaciolacustrine basin: Copper River, Alaska. Quaternary Science Reviews 21: 2237-2279.

Boothroyd, J.C.; Ashley, G.M. 1975. Processes, bar morphology, and sedimentary structures on braided outwash fans, Northeastern Gulf of Alaska. *In* Glaciofluvial and Glaciolacustrine sedimentation (Jopling, A.V.; McDonald, B.C.; editors). Society of Economic Paleontologists and Mineralogists, Special Publication 23: 193-222. Tulsa.

Boulton, G.S. 1986. Push moraines and glacier contact fans in marine and terrestrial environments. Sedimentology 33: 677-698.

Boulton, G.S. 1987. A theory of drumlin formation by subglacial sediment deformation. *In* Drumlin Symposium (Menzies, J.; Rose, J.; editors): 25-80. Balkema.

Benn, D.I. 1996. Subglacial and subaqueous processes near a glacier grounding line: sedimentological evidence from a former ice-dammed lake, Achnasheen, Scotland. Boreas 25: 23-36.

Benn, D.I.; Evans, D.J.A. 2010. Glaciers and Glaciation. Hodder Arnold Publication: 816 p. London.

Caldenius, C. 1932. Las glaciaciones Cuaternarias en la Patagonia y Tierra del Fuego. Geografiska Annaler 14A: 1-164.

Church, M.; Gilbert, R. 1975. Proglacial fluvial and lacustrine environments. *In* Glaciofluvial and Glaciolacustrine sedimentation (Jopling, A.V.; McDonald, B.C.; editors). Society of Economic Paleontologists and Mineralogists, Special Publication 23: 22-100. Tulsa.

Clague, J.J. 1975. Sedimentology and paleohydrology of Late Wisconsinan outwash, Rocky Mountain Trench, Southeastern British Columbia. *In* Glaciofluvial and Glaciolacustrine sedimentation (Jopling, A.V.; McDonald, B.C.; editors). Society of Economic Paleontologists and Mineralogists, Special Publication 23: 223-237. Tulsa.

Evans, D.J.A.; Hiemstra, J.H.; Ó Cofaigh, C. 2012. Stratigraphic architecture and sedimentology of a Late Pleistocene subaqueous moraine complex, southwest Ireland. Journal of Quaternary Science 27: 51-63.

Eyles, N.; Eyles, C.H.; Miall, A.D. 1983. Lithofacies types and vertical profile models; an alternative approach to the description and environmental interpretation of glacial diamict and diamictite sequences. Sedimentology 30: 393-410.

Eyles, N.; McCabe, A.M. 1989. Glaciomarine facies within subglacial tunnel valleys, the sedimentary record of glacio-isostatic downwarping in the Irish Sea Basin. Sedimentology 36: 431-448.

Fahnestock, R.K. 1963. Morphology and Hydrology of a glacial stream-White River, Mount Rainier, Washington. U.S. Geological Survey Profesional Paper 422-A: 70 p.

Fogwill, C.J.; Kubik, P.W. 2005. A glacial stage spanning the ACR in Torres del Paine (51), Chile, based on preliminary cosmogenic exposure ages. Geografiska Annaler 87A: 403-408.

Glasser, N.F.; Jansson, K.; Harrison, S.; Kleman, J. 2008. The glacial geomorphology and Pleistocene history of southern South America between 38ºS and 56ºS. Quaternary Science Reviews 27: 365-390.

García, J.L. 2012. Late Pleistocene ice fluctuations and glacial geomorphology of the Archipiélago de Chiloé, southern Chile. Geografiska Annaler 94A: 459-479.

García, J.L.; Kaplan, M.R.; Hall, B.H.; Schaefer, J.M.; Vega, R.V.; Schwartz, R.; Finkel, R. 2012. Glacial expansion in Southern Patagonia throughout the Antartic Cold Reversal. Geology 40: 859-862.

García, J.L.; Hall, B.L.; Kaplan, M.R.; Vega, R.M.; Strelin, J.A. 2014. Glacial geomorphology of the Torres del Paine region: Implications for glaciation, deglaciation and paleolake history. Geomorphology 204: 599-616.

Gravernor, C.P.; Von Brunn, V.; Dreimanis, A. 1984. Nature and classification of waterlain glacigenic sediments, exemplified by Pleistocene, Late Palaeozoic and Late Precambrian deposits. Earth Science Reviews 20: 105-166.

Gustavson, T.C. 1975. Sedimentation and Physical Limnology in Proglacial Malaspina Lake Southeastern Alaska. *In* Glaciofluvial and Glaciolacustrine sedimentation (Jopling, A.V.; McDonald, B.C.; editors). Society of Economic Paleontologists and Mineralogists, Special Publication 23: 249-263. Tulsa.

Hein, A.S.; Hulton, N.R.J.; Dunai, T.J.; Schnabel, C.; Kaplan, M.R.; Naylor, M.; Xu, S. 2009. Middle Pleistocene glaciation in Patagonia dated by cosmogenic-nuclide measurements on outwash gravels. Earth and Planetary Science Letters 286: 184-197.

Johnsen, T.F.; Brennand, T.A. 2006. The environment in and around ice-dammed lakes in the moderately high relief setting of the southern Canadian Cordillera. Boreas 35: 106-125.

Jopling, A.V. 1965. Hydraulic factors and the shape of laminae. Journal of Sedimentary Petrology 35: 777-791.

Kaplan, M.R.; Douglass, D.C.; Singer, B.S.; Ackert, R.P.; Caffee, M.W. 2005. Cosmogenic nuclide chronology of pre-last glacial maximum moraines at Lago Buenos Aires, 46ºS, Argentina. Quaternary Research 63: 301-315.

Mager, S.; Fitzsimons, S. 2007. Formation of glaciolacustrine Late Pleistocene end moraines in the Tasman Valley, New Zealand. Quaternary Science Reviews 26: 743-758.

Marden, C.J. 1993. Late Quaternary glacial history of the South Patagonia Icefield at Torres del Paine, Chile. Ph.D. Thesis (Unpublished), University of Aberdeen: 298 p.

Marden, C.J.; Clapperton, C.M. 1995. Fluctuations of the South Patagonian Icefield during the last glaciation and the Holocene. Journal of Quaternary Science 10: 197-210.

Marren, P.M. 2005. Magnitude and frequency in proglacial rivers: a geomorphological and sedimentological perspective. Earth Science Reviews 70: 203-251.

Matthews, J.A.; Cornish, R.; Shakesby, R.A. 1979. 'Saw-tooth' moraines in front of Bodalsbreen, southern Norway. Journal of Glaciology 22: 535-546.

McCabe, A.M.; Dardis, G.F.; Hanvey, P.M. 1984. Sedimentology of a Late Pleistocene submarine-moraine complex, County Down, Northern Ireland. Journal of Sedimentary Petrology 54: 716-730.

McKee, E.D. 1965. Experiments on ripple lamination. *In* Primary sedimentary structures and their hydrodynamic interpretation (Middleton, G.V.; editor). Society of Economic, Paleontologists Mineralogists, Special Publication 12: 66-83.

Moreno, P.I.; Kaplan, M.R.; François, J.P.; Villa-Martínez, R.; Moy, C.M.; Stern, C.R.; Kubik, P.W. 2009. Re-newed glacial activity during the Antarctic cold reversal and persistence of cold conditions until 11.5 ka in southwestern Patagonia. Geology 37: 375-378.

Reineck, H.E.; Singh, I.B. 1980. Depositional sedimentary environments. Springer-Verlag, Berlin Heilderberg: 554 p.

Sagredo, E.A.; Moreno, P.I.; Villa-Martínez, R.; Kaplan, M.R.; Kubik, P.W.; Stern, C.R. 2011. Fluctuations of the Última Esperanza ice lobe (52°S), Chilean Patagonia, during the last glacial maximum and termination 1. Geomorphology 125: 92-108.

Solari, M.A.; Le Roux, J.P.; Hervé, F.; Airo, A.; Calderón, M. 2012. Evolution of the Great Tehuelche Paleolake in the Torres del Paine National Park of the Chilean Patagonia during the last glacial maximum and Holocene. Andean Geology 39 (1): 1-21. doi: 10.5027/andgeoV39N1-a01.

Stern, C.R. 1990. The tephrochronology of southernmost Patagonia. National Geographic Research 6: 110-126.

Stern, C.R. 2004. Active Andean volcanism: its geologic and tectonic setting. Revista Geológica de Chile 31 (2): 161-206. doi: 10.5027/andgeoV31n2-a01.

Stern, C.R. 2008. Holocene tephrochronology record of large explosive eruptions in the southernmost Patagonia Andes. Bulletin of Volcanology 70: 435-454.

Stern, C.R.; Moreno, P.I.; Villa-Martínez, R.; Sagredo, E.A.; Prieto, A.; Labarca, R. 2011. The late-glacial R1 eruption of Reclus volcano, Andean Austral Volcanic Zone: implications for evolution of ice-dammed proglacial lakes in Ultima Esperanza, Chile. Andean Geology 38 (1): 82-97. doi: 10.5027/andgeoV38n1-a06.

Strelin, J.A.; Denton, G.H.; Vandergoes, M.J.; Ninnemann, U.S.; Putnam, A.E. 2011. Radiocarbon chronology of the late-glacial Puerto Bandera moraines, Southern Patagonian Icefield, Argentina. Quaternary Science Reviews 30: 2551-2569.

Sugden, D.E.; Bentley, M.J.; Fogwill, C.J.; Hulton, N.R.J.; McCulloch, R.D.; Purves, R.S. 2005. Late-glacial glacier events in southernmost South America: a blend of 'northern' and 'southern' hemispheric climatic signals? Geografiska Annaler 87A: 273-288.

Thomas, G.S.P.; Connell, R.J. 1985. Iceberg drop. Dump and grounding structures from Pleistocene lacustrine sediments, Scotland. Journal of Sedimentary Petrology 55: 243-249.

Turbek, S.E.; Lowell, T.V. 1999. Glacial deposition along an ice-contact slope: an example from the southern Lake District, Chile. Geografiska Annaler 81A: 325-346.

Manuscript received: November 09, 2014; revised/accepted: April 15, 2015; available online: April 27, 2015.